Topological spin-polarized electron layer above the surface of Ca-terminated Bi_{2}Se_{3}

Xiaoxiong Wang, Guang Bian, T. Miller, and T.-C. Chiang

Phys. Rev. B **87**, 035109 — Published 7 January 2013

DOI: 10.1103/PhysRevB.87.035109

Topological Spin-Polarized Electron Layer above the Surface of Ca-Terminated Bi_2Se_3

Xiaoxiong Wang,[1,2,3] Guang Bian,[2,3] T. Miller,[2,3,4] and T.-C. Chiang[2,3,4]

[1]College of Science, Nanjing University of Science and Technology, Nanjing 210094, China

[2]Department of Physics, University of Illinois at Urbana-Champaign, 1110 West Green Street, Urbana, Illinois 61801-3080, USA

[3]Frederick Seitz Materials Research Laboratory, University of Illinois at Urbana-Champaign, 104 South Goodwin Avenue, Urbana, Illinois 61801-2902, USA

[4]Synchrotron Radiation Center, University of Wisconsin-Madison, 3731 Schneider Drive, Stoughton, WI 53589-3097, USA

PACS numbers: 71.70.Ej, 73.20.At, 79.60.Dp

ABSTRACT

Spin-polarized gapless surface states on the boundary of topological insulators are of interest for spintronic applications. First-principles calculations show that adsorption of a Ca monolayer on films of the prototypical topological insulator, Bi_2Se_3, yields a substantial enhancement of the surface-state spin polarization, despite the low atomic mass of Ca and its weak spin-orbit coupling. Much of the topological surface electron distribution is transferred outside the Ca to form a polarized electron layer out in vacuum; this spatial separation from the substrate minimizes scattering by defects in Bi_2Se_3 and can be a useful feature for device engineering.

I. INTRODUCTION

Topological insulators are a new class of materials with unusual surface and interface properties that are well suited for high-efficiency spin information transport and processing [1-5]. These materials contain high-Z elements with strong spin-orbit coupling to yield a symmetry-inverted bulk band gap [6, 7]. When a topological insulator and an ordinary insulator are joined to form an interface, the symmetry reversal in crossing the interface must result in gap closing [8, 9]. This topological effect gives rise to spin-polarized gapless surface states when the ordinary insulator is empty space or vacuum [10-12]. These states are of special interest for spintronic applications [13, 14]. However, their spin polarization is generally less than 100%, and methods to improve the spin polarization and spin current (device signal strength) are of interest. Chemisorption or deposition is the simplest, but very effective, method to engineer the surface states and achieve desirable properties.

Chemisorption of low-Z elements on a topological insulator is expected, intuitively, to leave the surface spin texture largely intact because of the adsorbate's weak spin-orbit interaction, but this is not so as we shall demonstrate. Our studies are motived in part by the fact that pristine surfaces are generally irrelevant to device applications. Chemisorption, being a key device fabrication process and the first step in interface formation, presents a simple case to establish the basic trends. Our first-principles calculation results reveal that Ca adsorption on films of Bi_2Se_3 yields a strong effect, much more so than Na and Al with valencies bracketing that of Ca. Part of the topological surface electron distribution is transferred outside the adsorbate layer, resulting in a polarized electron layer out in vacuum. The reduced overlap of the spin conduction channel with possible substrate defects (such as vacancies, antisites, impurities, and interstitials),

the interface, and other conducting channels can be very beneficial to spin transport. Our work elucidates why Ca is special, and suggests a general principle for surface engineering.

II. COMPUTATIONAL METHODS

Our first-principles calculations were performed using the Abinit package [15, 16] and Hartwigsen-Goedecker-Hutter pseudopotentials [17] within the LDA approximation. The cutoff energy was 400 eV. A supercell geometry was employed. For films chemisorbed on one face, the supercell consisted of two identical films arranged as twin images in order to cancel out the unphysical electric field within the vacuum gap. Each vacuum gap was chosen to be at least 15 Å. The atomic positions of the adsorbates and the top quintuple layer were allowed to relax until the residual forces on the atoms became less than 2×10^{-5} hartree/bohr. A slight asymmetry involving displacing the bottommost atomic layer downward by 0.01 Å was introduced into each slab without the adlayers in order to break the degeneracy and separate out the states associated with the two faces of pristine Bi_2Se_3 films. The same displacement is applied to just one of the two twin slabs with the adlayers in a supercell to lift the degeneracy between the two twin slabs. The displacement has little effect otherwise on the electronic band structure.

III. RESULTS AND DISCUSSION

A. Evolution of the topological surface states in Bi_2Se_3 films upon chemisorption

The compound Bi_2Se_3 is the best studied topological insulator [18-25]. Its structure consists of quintuple layers (QLs), with each QL made of three Se atomic layers intercalated by two Bi atomic layers, as indicated in Figs. 1(a) and 1(b) [18]. The topological surface states of Bi_2Se_3, with a decay length of ~1 QL, are essentially in the bulk limit at a film thickness of 6 QLs based on

prior experimental and theoretical work [19, 26]. The calculated electronic structure of a 6-QL film is shown in Figs. 2(a) and 2(b), where the green- and yellow-shaded areas represent the projected bulk band regions and the gap, respectively. Bridging the gap are two surface bands intersecting at $\bar{\Gamma}$ to form a Dirac point [20], labeled P_0 and P_0' for the states localized at the top and bottom faces of the film, respectively. The color coding shows the normalized charge moment defined by

$$M = \frac{2}{D}\int \rho(z) z dz \tag{1}$$

where D is the film thickness, $\rho(z)$ is the normalized planar charge density, and $z = 0$ is at the center of the film. Saturated red (blue) color corresponds to $M = +1$ (–1), or a charge distribution fully concentrated at the top (bottom) face of the film; while white color corresponds to $M = 0$ for a charge distribution spread out in the film characteristic of quantum well states. The surface states become quantum well states as they enter the projected bulk band regions [27].

The normalized spin polarization

$$\sigma_y \equiv \langle \psi | \frac{2s_y}{\hbar} | \psi \rangle \tag{2}$$

is shown in Figs. 2(e) and 2(f) for the surface states at the top and bottom faces, respectively, using a similar color coding scheme. The spin polarizations for the top and bottom faces are equal in magnitude but opposite in direction; the extreme values, ±65% as indicated by the triangular marks next to the color scale bar, occur near the zone center and are much less than ±100% [21]. They decay to ~0 in the bulk band regions, where quantum-well states must occur in spin-degenerate pairs by virtue of inversion symmetry of the film [27].

We have considered the chemisorption of a number of elements in the periodic table. The results for Ca and Cl adsorbed on the top face of a 6-QL Bi_2Se_3 film are presented here, which

illustrate the wide range of behavior for adsorbates with very different electronegativities. The calculated adsorption geometry for Cl is on top of each surface Se atom at a bond length of 2.23 Å and an adsorption energy of 1.93 eV, while each Ca adatom sits in a 3-fold hollow site at 1.39 Å above the top Se atomic plane with an adsorption energy of 1.44 eV. The structures are indicated in Figs. 1(c)-1(f). The corresponding electronic band structures are presented in Figs. 2(c) and 2(g) for Ca adsorption, and 2(d) and 2(h) for Cl adsorption.

The Cl case is simpler and provides a baseline for comparison. Upon moving an isolated Cl atomic layer adiabatically from vacuum to the final chemisorption position, calculations show that the surface states on the bottom face of the film and the associated Dirac point P_0' remain intact. The original Dirac point P_0 associated with the top face is shifted downward into the valence band region to become L_1 as labeled in Fig. 2(d). Part of the upper branch of L_1 remains within the bulk gap and reaches the zone boundary at $\overline{M}$, where it meets its time-reversal partner dragged down from the conduction band to form a Dirac point L_2 at $\overline{M}$. The two Dirac points P_0' and L_2 are connected, but each face of the film has just one set of topological surface bands spanning the gap. The bands connecting P_0' and L_2 remain spin polarized within the bulk band regions because of the breakdown of inversion symmetry by adsorption.

Chemisorption of Ca on the top face, by contrast, is much more interesting. The Dirac point P_0' at the bottom face remains intact. The top face now has two Dirac points; the original Dirac point P_0 evolves into A_1, while A_2 is derived from Ca states in conjunction with the conduction band states of Bi_2Se_3 [Figs. 2(c) and 2(g)]. With the Fermi level placed in the middle of the bulk band gap, it crosses the surface bands at the top face three times; an odd number of crossings is required by the topological order. The maximum spin polarizations of the new

surface states associated with A_1 also occur near the zone center but are much stronger than the pristine case (±0.82 vs. ±0.65).

This polarization boost is best illustrated in Fig. 3(a) by the spin-resolved planar charge density for the upper state in each pair close to the Dirac point (the lower state has the same charge density but opposite spin polarization). For the pristine film, the surface states associated with P_0 and P_0' have a decay length of just about 1 QL; the one associated with P_0' remains little affected by Ca adsorption. The state associated with A_2 shows a more diffuse wave function and is otherwise unremarkable. The state associated with A_1, derived from P_0, shows a strongly spin-polarized charge peak outside the Ca atomic plane, and the net spin polarization of the state is much enhanced relative to the pristine case. This observation is interesting; because Ca has a negligible spin-orbit coupling, it is not expected, intuitively, to affect the surface spin texture directly. A close inspection reveals that the charge peak associated with A_1 is derived from the Ca 4p_z state. It is accompanied by a dip in the charge density on the opposite side of the Ca atomic plane (indicated by a triangle in Fig. 3(a)). This dip arises from destructive interference between the Ca 4p_z and the substrate states (mostly Se 4p); the underlying electronic hybridization gives rise to the strongly polarized Ca 4p_z lobe out in vacuum.

The case gets more pronounced for thinner films . The smallest film thickness for which surface states associated with the two faces can still be separately identified is 2 QLs. At this thickness, the surface states of the two faces overlap to form a tunneling gap of 0.06 eV at P_0, which is evident in Figs. 4(a) and 4(b). The dispersion relations near the zone center become rounded, rather than linear. The charge moment and the spin polarization near the zone center are much reduced compared to the pristine 6-QL case because of partial charge overlap and partial spin cancellation. With Ca adsorption, the tunneling gap vanishes, as seen in Figs. 4(c) and 4(g),

because of the asymmetry of the system, while the linear dispersion relation near the zone center is restored. The spin polarization of the surface states associated with A_1 becomes much stronger after Ca adsorption, by a factor of 2.6 (0.78 vs. 0.3). The suppression of the tunneling gap and the enhancement of the spin polarization are both desirable features for spin transport. The charge peak out in vacuum and its destructive-interference dip are evident in Fig. 3(b). The charge peak appears as a rippled layer in three dimensions, as shown in Fig. 3(c), because of in-plane interaction. The charge moment and spin polarization of the states associated with P_0' at the bottom face are also much enhanced for both Ca and Cl chemisorption to values close to the thick-film limit as evidenced by a comparison between Figs. 2 and 4. This is because the asymmetry in the system eliminates the cancellation effect involving the two faces.

B. Mechanism for the spin polarization enhancement in Ca-terminated Bi_2Se_3

Calculations for Na and Al, with chemical valencies bracketing that of Ca, reveal a similar polarized electron density peak out in vacuum, but the effect is not as impressive. The reason is that Ca has its 4*s* level nominally filled. Hybridization brings the $4p_z$ state into the band gap with a strong spin polarization. This effect is reduced for Na, as its partially empty 3*s* level should be the dominant contributor to the surface states in the gap. For Al, the $3p_z$ orbital is already partially occupied, and further occupancy of the orbital can lead to spin pairing and a less dramatic effect. By contrast, chemisorption of Cl yields an almost full Cl 3*p* level with its spectral weight mostly distributed below the band gap and little for the surface states in the gap.

The transfer of the spin-polarized topological electron density into vacuum in Ca-Bi_2Se_3 can be very beneficial to spin transport. Because of the reduced overlap of the wave function of the surface state with the substrate, scattering by defects in the substrate and coupling to the interface are significantly suppressed. The reduced spatial overlap with the other states, bulk or surface

[see Figs. 3(a) and 3(b) for an example], minimizes the crosstalk between conduction channels. These findings are relevant to engineering concepts involving topological surface states. Furthermore, both the top and bottom faces of a thin film can be chemically modified. For example, the Fermi level could be tuned to the desired position by chemically manipulating the bottom face of the film.

C. Quantum confinement effect on the topological surface states

The band structure and charge moment of Ca-adsorbed Bi_2Se_3 are shown in Fig. 5 for each Bi_2Se_3 film thickness in the 2-6 QL range. Note that the Dirac point P_0' has a higher energy than A_1 for the 6-QL substrate (Fig. 2), but this energy ordering is reversed for the 2-QL substrate (Fig. 4). It is interesting to determine where the crossover occurs. The calculated band structure alone does not quite tell the story convincingly. The calculated charge moment is crucial for tracking the states associated with the top and bottom faces. In Fig. 5, (a)-(d) correspond to 2-5 QL films, but for simplicity and consistency, the structural parameters are assumed to be fixed based on the 2-QL film; (e) and (f) are for 5- and 6-QL films with structural parameters based on the 6-QL film. Results in (d) and (e), both for a 5-QL film but with different assumed structural parameters, are very close; thus, structural relaxation does not play an important role as further verified by additional calculations. From Fig. 5, we can conclude that the crossover of P_0' and A_1 occurs between 2 and 3 QLs. This crossover can be attributed to quantum confinement that affects the various states in different ways.

IV. CONCLUDING REMARKS

Spin polarization, spin current, and charge distribution are key figures of merit for the utility of topological states in devices. Our work demonstrates viable routes, taking advantage of the orbital symmetry and electron population of adsorbate atoms, for surface engineering to modify or improve these properties, and the atomic-level understanding of the interfacial interaction is of basic interest. Low-Z elements do not affect the spin texture directly by spin-orbit coupling near their cores; rather, orbital hybridization with the topological states yields the desired modification. The net interaction is an indirect spin-orbit coupling, akin to the indirect exchange for magnetic systems. Another important effect is the modification of the tunneling gap, which can affect transport at very small film thicknesses of interest to nanoscale device integration.

ACKNOWLEDGMENTS

This work was supported by the U.S. Department of Energy, Office of Science (grant DE-FG02-07ER46383 for TCC), the National Natural Science Foundation of China (No. 11204133 for XW), the Jiangsu Province Natural Science Foundation of China (No. BK2012393 for XW), and the Young Scholar Project of NUST (No. AB41382 for XW). GB acknowledges partial support by the Yee Memorial Fund Fellowship.

REFERENCES

[1] C. L. Kane and E. J. Mele, Science **314**, 1692 (2006).

[2] D. Hsieh, D. Qian, L. Wray, Y. Xia, Y. S. Hor, R. J. Cava, and M. Z. Hasan, Nature **452**, 970 (2008).

[3] M. Z. Hasan and C. L. Kane, Rev. Mod. Phys. **82**, 3045 (2010).

[4] X.-L. Qi and S.-C. Zhang, Rev. Mod. Phys. **83**, 1057 (2011).

[5] J. E. Moore, Nature **464**, 194 (2010).

[6] B. A. Bernevig, T. L. Hughes, and S. C. Zhang, Science **314**, 1757 (2006).

[7] M. König, S. Wiedmann, C. Brüne, A. Roth, H. Buhmann, L. W. Molenkamp, X.-L. Qi, and S.-C. Zhang, Science **318**, 766 (2007).

[8] L. Fu and C. L. Kane, Phys. Rev. B **76**, 045302 (2007).

[9] T. Zhang, P. Cheng, X. Chen, J.-F. Jia, X. Ma, K. He, L. Wang, H. Zhang, X. Dai, Z. Fang, X. Xie, and Q.-K. Xue, Phys. Rev. Lett. **103**, 266803 (2009).

[10] D. Hsieh, Y. Xia, L. Wray, D. Qian, A. Pal, J. Dil, J. Osterwalder, F. Meier, G. Bihlmayer, C. Kane, Y. S. Hor, R. J. Cava, and M. Z. Hasan, Science **323**, 919 (2009).

[11] P. Roushan, J. Seo, C. V. Parker, Y. S. Hor, D. Hsieh, D. Qian, A. Richardella, M. Z. Hasan, R. J. Cava, and A. Yazdani, Nature **460**, 1106 (2009).

[12] Z. H. Pan, E. Vescovo, A. V. Fedorov, D. Gardner, Y. S. Lee, S. Chu, G. D. Gu, and T. Valla, Phys. Rev. Lett. **106**, 257004 (2011).

[13] J. Sinova and I. Žutić, Nat. Mater. **11**, 368 (2012).

[14] D. Pesin and A. H. MacDonald, Nat. Mater. **11**, 409 (2012).

[15] X. Gonze, G.-M. Rignanese, M. Verstraete, J.-M. Beuken, Y. Pouillon, R. Caracas, F. Jollet, M. Torrent, G. Zerah, M. Mikami, P. Ghosez, M. Veithen, J.-Y. Raty, V. Olevano, F.

Bruneval, L. Reining, R. Godby, G. Onida, D. R. Hamann, and D. C. Allan, Z. Kristallogr. **220**, 558 (2005).

[16] X. Gonze, B. Amadon, P.-M. Anglade, J.-M. Beuken, F. Bottin, P. Boulanger, F. Bruneval, D. Caliste, R. Caracas, M. Côté, T. Deutsch, L. Genovese, P. Ghosez, M. Giantomassi, S. Goedecker, D. R. Hamann, P. Hermet, F. Jollet, G. Jomard, S. Leroux, M. Mancini, S. Mazevet, M. J. T. Oliveir, G. Onida, Y. Pouillon, T. Rangel, G.-M. Rignanese, D. Sangalli, R. Shaltaf, M. Torrent, M. J. Verstraete, G. Zerah, and J. W. Zwanziger, Comput. Phys. Commun. **180**, 2582 (2009).

[17] C. Hartwigsen, S. Goedecker, and J. Hutter, Phys. Rev. B **58**, 3641 (1998).

[18] H. Zhang, C. X. Liu, X. L. Qi, X. Dai, Z. Fang, and S. C. Zhang, Nat. Phys. **5**, 438 (2009).

[19] Y. Zhang, K. He, C.-Z. Chang, C.-L. Song, L.-L. Wang, X. Chen, J.-F. Jia, Z. Fang, X. Dai, W.-Y. Shan, S.-Q. Shen, Q. Niu, X.-L. Qi, S.-C. Zhang, X.-C. Ma, and Q.-K. Xue, Nat. Phys. **6**, 584 (2010).

[20] Y. Xia, D. Qian, D. Hsieh, L.Wray, A. Pal, H. Lin, A. Bansil, D. Grauer, Y. S. Hor, R. J. Cava, and M. Z. Hasan, Nat. Phys. **5**, 398 (2009).

[21] O. V. Yazyev, J. E. Moore, and S. G. Louie, Phys. Rev. Lett. **105**, 266806 (2010).

[22] K. Kuroda, M. Arita, K. Miyamoto, M. Ye, J. Jiang, A. Kimura, E. Krasovskii, E. Chulkov, H. Iwasawa, T. Okuda, K. Shimada, Y. Ueda, H. Namatame, and M. Taniguchi, Phys. Rev. Lett. **105**, 076802 (2010).

[23] P. Cheng, C. Song, T. Zhang, Y. Zhang, Y. Wang, J. F. Jia, J. Wang, B. F. Zhu, X. Chen, X. Ma, K. He, L. Wang, X. Dai, Z. Fang, X. Xie, X. L. Qi, C. X. Liu, S. C. Zhang, and Q. K. Xue, Phys. Rev. Lett. **105**, 076801 (2010).

[24] P. D. C. King, R. C. Hatch, M. Bianchi, R. Ovsyannikov, C. Lupulescu, G. Landolt, B. Slomski, J. H. Dil, D. Guan, J. L. Mi, E. D. L. Rienks, J. Fink, A. Lindblad, S. Svensson, S. Bao, G. Balakrishnan, B. B. Iversen, J. Osterwalder, W. Eberhardt, F. Baumberger, and P. Hofmann, Phys. Rev. Lett. **107**, 096802 (2011).

[25] Z.-H. Zhu, G. Levy, B. Ludbrook, C. N. Veenstra, J. A. Rosen, R. Comin, D. Wong, P. Dosanjh, A. Ubaldini, P. Syers, N. P. Butch, J. Paglione, I. S. Elfimov, and A. Damascelli, Phys. Rev. Lett. **107**, 186405 (2011).

[26] O. V. Yazyev, E. Kioupakis, J. E. Moore, and S. G. Louie, Phys. Rev. B **85**, 161101(R) (2012).

[27] G. Bian, T. Miller, and T. C. Chiang, Phys. Rev. Lett. **107**, 036802 (2011).

FIG. 1. (color online). Top views of the atomic structures of (a) Bi_2Se_3, (c) Bi_2Se_3-Ca, and (e) Bi_2Se_3-Cl. The corresponding side views are shown in (b), (d), and (f), respectively; only the topmost quintuple layer is included. A quintuple layer unit cell is indicated in (b) with the dotted rectangle.

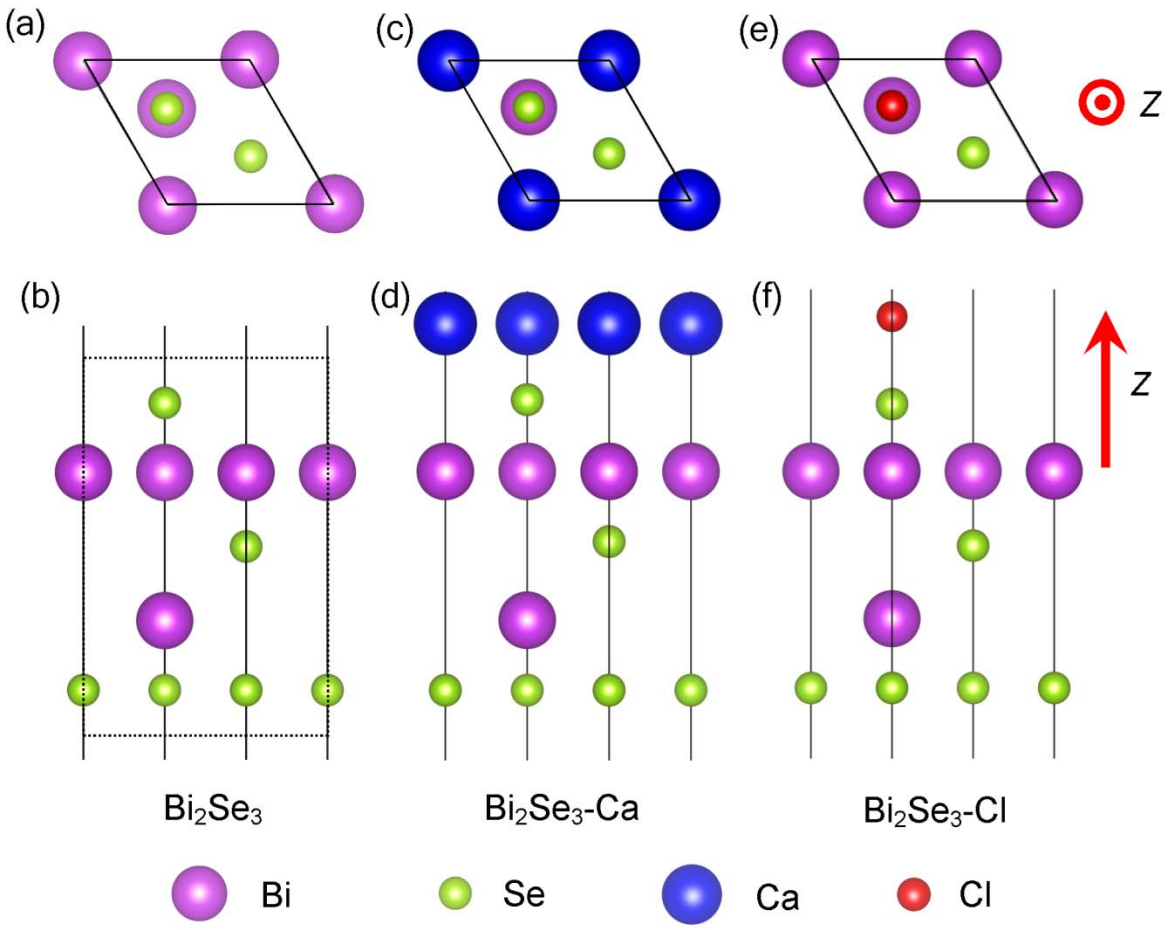

FIG. 2. (color online). Band dispersions with normalized charge moment *M* (upper row) and spin polarization σ_y (lower row) indicated by color coding for the surface states and nearby quantum well states. (a) and (e) are for the top surface states of a pristine 6-QL film, while (b) and (f) are for the bottom surface states of the same film. (c) and (g) are for Ca chemisorption on the top face of the film, and (d) and (h) are for Cl chemisorption on the top face of the film. The green- and yellow-shaded areas indicate the projected bulk band regions and gaps, respectively. The maximum $\pm\sigma_y$ for the topological surface states of the pristine film are shown with triangles next to the lower color scale bar.

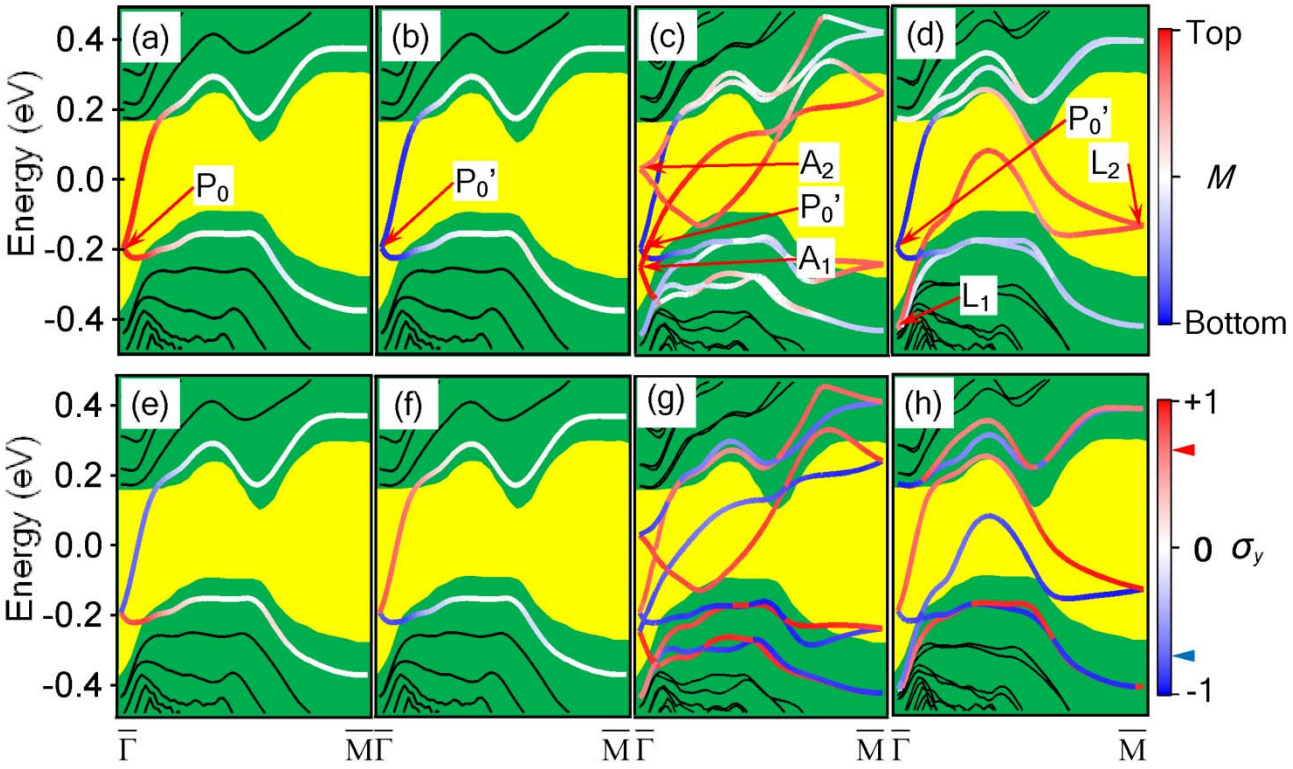

FIG. 3. (color online). (a) Spin-resolved charge distributions for the upper state near each Dirac point indicated in Fig. 2 for pristine and Ca- and Cl-chemisorbed 6-QL Bi_2Se_3 films. The curves indicate the total charge density, and the red-white-blue color coding indicates the spin polarization $\sigma_y(z)$. The boundaries of the quintuple layers are marked by vertical dash-dotted lines. The positions of the atomic planes of Ca and Cl are marked by solid vertical lines. The red triangle indicates the interference minimum in the charge density. (b) Same as (a) except that the Bi_2Se_3 film thickness is 2 QLs. (c) Three-dimensional isosurface of charge distribution of state A_1 for a Ca-adsorbed 2-QL Bi_2Se_3 film in a 3×3 unit cell. The atomic positions are indicated. The charge layer above the Ca atoms is evident.

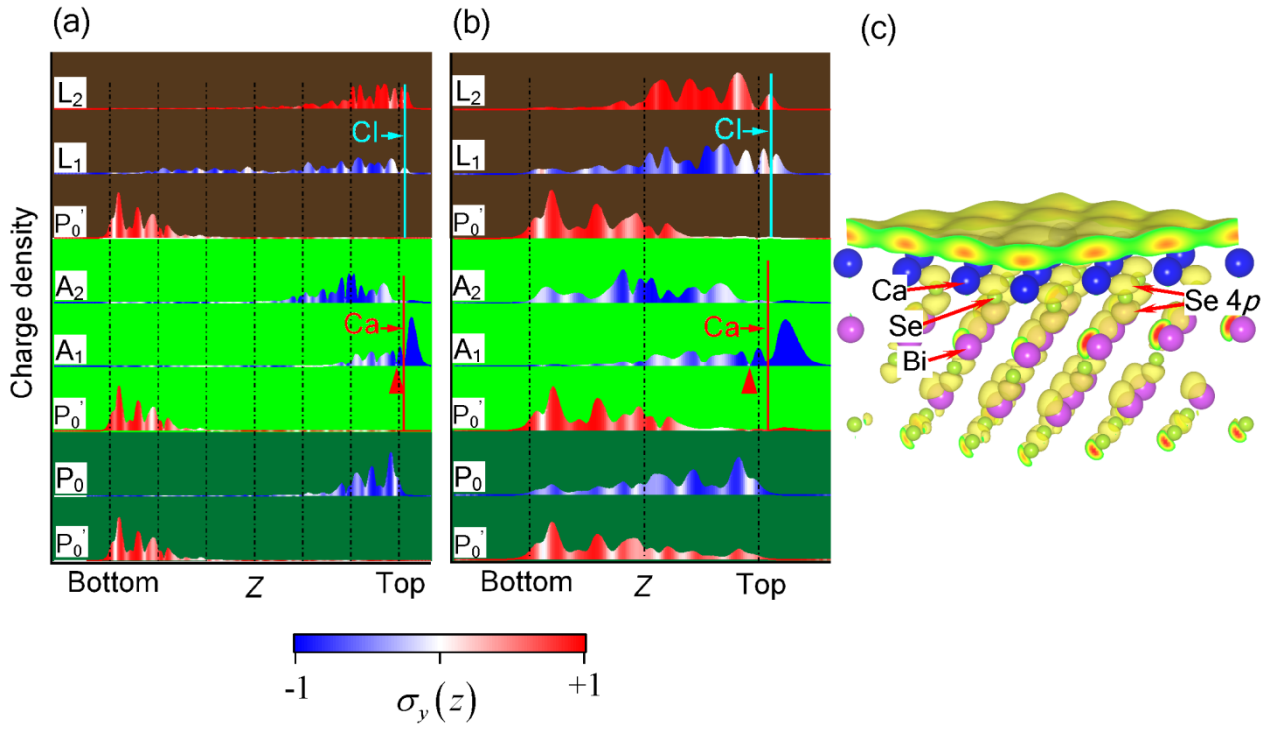

FIG. 4. (color online). Same as Fig. 2 except that the Bi_2Se_3 film has a thickness of 2 instead of 6 QLs.

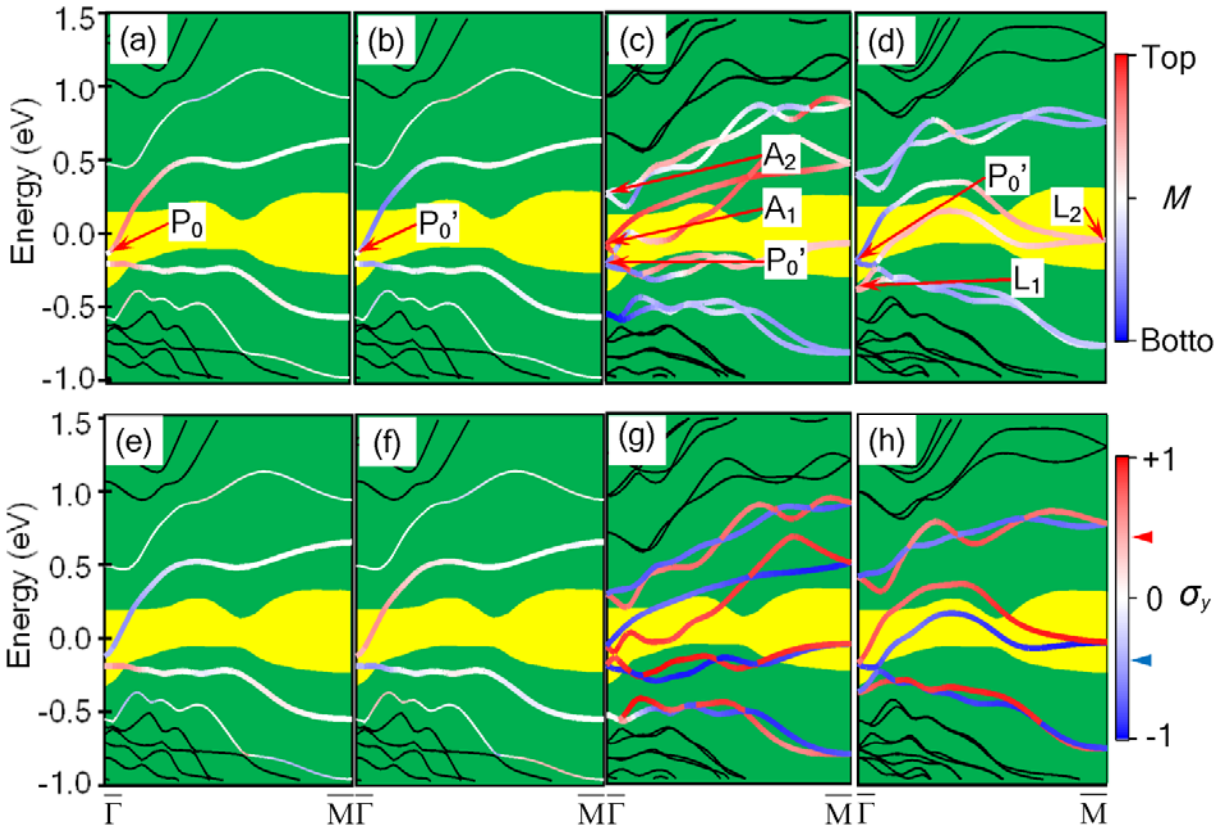

Fig. 5. (color online). Band structure and charge moment of Ca-adsorbed Bi_2Se_3 for each Bi_2Se_3 film thickness in the 2-6 QL range. The green- and yellow-shaded areas indicate the projected bulk band regions and the bulk gap, respectively. The color coding indicates the charge moment *M*. The Bi_2Se_3 substrate thicknesses for (a)-(d), (e), and (f) are 2-5, 5, and 6 QLs, respectively. (a)-(d) are based on the optimized geometrical structure of 2-QL Bi_2Se_3-Ca; (e) and (f) are based on the optimized geometrical structure of 6-QL Bi_2Se_3-Ca. Dirac points P_0' and A_1 are indicated.